Tomasch Oscillations as Above-Gap Signature of Topological Superconductivity

Antonio Štrkalj,[2,*,‡] Xi-Rong Chen,[1,3,*] Wei Chen,[1,†] D. Y. Xing,[1] and Oded Zilberberg[4]
[1]*National Laboratory of Solid State Microstructures, School of Physics, and Collaborative Innovation Center of Advanced Microstructures, Nanjing University, Nanjing 210093, China*
[2]*TCM Group, Cavendish Laboratory, J. J. Thomson Avenue, Cambridge CB3 0HE, United Kingdom*
[3]*School of Microelectronics and Physics, Hunan University of Technology and Business, Changsha, Hunan Province 410205, China*
[4]*Department of Physics, University of Konstanz, 78464 Konstanz, Germany*

(Received 16 May 2023; revised 3 October 2023; accepted 8 January 2024; published 7 February 2024)

The identification of topological superconductors usually involves searching for in-gap modes that are protected by topology. However, in current experimental settings, the smoking-gun evidence of these in-gap modes is still lacking. In this Letter, we propose to support the distinction between two-dimensional conventional s-wave and topological p-wave superconductors by above-gap transport signatures. Our method utilizes the emergence of Tomasch oscillations of quasiparticles in a junction consisting of a superconductor sandwiched between two metallic leads. We demonstrate that the behavior of the oscillations in conductance as a function of the interface barriers provides a distinctive signature for s-wave and p-wave superconductors. Specifically, the oscillations become weaker as the barrier strength increases in s-wave superconductors, while they become more pronounced in p-wave superconductors, which we prove to be a direct manifestation of the pairing symmetries. Our method can serve as a complimentary probe for identifying some classes of topological superconductors through the above-gap transport.

DOI: 10.1103/PhysRevLett.132.066301

Introduction.—At the heart of superconductivity is the pairing of conduction electrons into Cooper pairs that form a bosonic condensate [1]. These Cooper pairs can be in either a spin-singlet state, with a total spin 0, or a spin-triplet state, with a spin 1. The spin-singlet state is characterized by a wave function with even angular momentum, such as s-wave or d-wave, while the spin-triplet state supports a wave function with odd angular momentum, such as p-wave or f-wave. In conventional s-wave superconductivity the pairing function $\Delta(\mathbf{k}) = \Delta_s$ is constant irrespective of the direction of the momentum vector $\mathbf{k}$. The Cooper pair, in this case, consists of two electrons with opposite spins. On the other hand, in unconventional p-wave superconductors, electrons with the same spin form Cooper pairs and the pairing $\Delta(\mathbf{k})$ is no longer constant with $\mathbf{k}$ [2–7].

Over the past several decades, there has been significant interest in unconventional p-wave superconductors [2–5,7,8], mostly due to their unique topological properties [9–11]. The topology implies, for example, the presence of exotic quasiparticles, such as Majorana zero-energy modes in one-dimensional systems [12,13], and in-gap Majorana states in two-dimensional systems [14–20]. These quasiparticles have potential applications in topological quantum computing [21–23], and are used as a key signature for discerning between topologically nontrivial p-wave and trivial s-wave superconductors. As a result, the search for topological superconductors encompass two main approaches. The first approach involves searching for topological superconductivity in specific materials, such as Sr_2RuO_4 [3,24–26], UTe_2 [27], Pb_3Bi [28], and hybrid systems such as Pb/Co/Si(111) [20,29]. The second approach involves using engineered metamaterials that share some of the properties of topological superconductors [9,19,30–41].

The behavior of superconductors can be largely understood through the Bogoliubov–de Gennes (BdG) formalism [42], which describes the mean-field behavior of quasiparticles in the superconductor that form through hybridization between electrons and holes. The resulting band structure resembles a "sombrero" shape, with an energy gap that depends on the details of the pairing function $\Delta(\mathbf{k})$. Notably, the band structure of quasiparticles in superconductors resembles that of band-inverted semiconductors [43–46], with the band gap of the latter corresponding to the superconducting gap in the former. Recently, Fabry-Pérot oscillations were observed in a two-dimensional junction made out of an inverted InAs/GaSb double quantum well [46]. The mechanism leading to such Fabry-Pérot oscillations in a two-dimensional junction stems from the sombrero-shaped band structure. Specifically, the interference is dominated by the scattering between the electronlike and holelike states at energies close to the band gap [46,47]. Such interference is quite ubiquitous and applies to a variety of condensed matter systems with inverted-band dispersions [46,48]. Interestingly, similar Fabry-Pérot oscillations are also studied in superconducting junctions and go under the name of Tomasch oscillations [49–55].

In this Letter, we demonstrate that Tomasch oscillations in the conductance across the two-dimensional NSN junctions (two normal metals sandwiching a superconductor) provide a signature that can act as a complementary probe to discern between conventional and topological superconductors. As such, we focus on transport with energies above the superconducting gap and investigate the effects of the interface barriers on the Tomasch oscillations for superconductors with different pairing symmetries. In the weak barrier limit, we find that the inverted-band mechanism responsible for the oscillations is the same for both s-wave and p-wave superconductors. Interestingly, the oscillations are crucially different in the strong barrier limit, i.e., in the tunneling limit. This distinction arises from differing pairings in the BdG Hamiltonians of s- and p-wave superconductors, affecting the visibility of the oscillations. Our result offers an alternative experimental probe using the *above-gap* transport signatures for distinguishing between conventional and topological superconductors, in contrast to the commonly studied in-gap signatures [56].

Setup.—We study a two-dimensional NSN junction made of two normal metals (N) and a superconductor (S) sandwiched between them; see Fig. 1(a). We concentrate on a ballistic case, where the mean free path of particles is the largest scale in the system. The BdG Hamiltonian around Γ point in the continuum limit of the whole system is

$$H = H_\mathrm{N} + H_\mathrm{S} + U(x)\sigma_z, \qquad (1)$$

where the Pauli matrix σ_z (and later σ_x) operates in the Nambu space and H_N describes the metallic leads

$$H_\mathrm{N}(\mathbf{k}) = \begin{pmatrix} \frac{\hbar^2}{2m_\mathrm{N}}\mathbf{k}^2 - \mu_\mathrm{N} & 0 \\ 0 & -\frac{\hbar^2}{2m_\mathrm{N}}\mathbf{k}^2 + \mu_\mathrm{N} \end{pmatrix}, \qquad (2)$$

with $\mathbf{k} = (k_x, k_y)$ the wave vector, m_N the effective mass of electrons in the metallic leads, and μ_N their chemical potential. The Hamiltonian of the superconductor is given by [57]

$$H_\mathrm{S}(\mathbf{k}) = \begin{pmatrix} \frac{\hbar^2}{2m_\mathrm{S}}\mathbf{k}^2 - \mu_\mathrm{S} & \Delta(\mathbf{k}) \\ \Delta^*(\mathbf{k}) & -\frac{\hbar^2}{2m_\mathrm{S}}\mathbf{k}^2 + \mu_\mathrm{S} \end{pmatrix}, \qquad (3)$$

with m_S and μ_S the corresponding effective mass and chemical potential, respectively. We introduce a pairing potential $\Delta(\mathbf{k})$ corresponding to two types of superconductors, namely a time-reversal symmetric s-wave superconductor with a constant pairing $\Delta(\mathbf{k}) = \Delta_s$, and a time-reversal broken p-wave superconductor with $\Delta(\mathbf{k}) = i\Delta_p(k_x + ik_y)$. Note that for a vanishing pairing potential, the band structure takes a parabolic shape. Furthermore, at the N-S interfaces, we introduce sharp barriers $U(x) = U[\delta(x) + \delta(x - L)]$ to account for the materials' mismatch or imperfections [58,59]. Alternatively, the barriers can be introduced and adjusted by local strip gates. For simplicity, we assume that the barriers are perfectly flat in the y direction, such that they do not break the translational invariance in the y direction. In the following, we employ the often-used dimensionless barrier strength $Z \equiv mU/(\hbar^2 k_\mathrm{F})$ and, without loss of generality consider $m \equiv m_\mathrm{N} = m_\mathrm{S}$ and $\mu \equiv \mu_\mathrm{N} = \mu_\mathrm{S} = \hbar^2 k_\mathrm{F}^2/(2m)$.

We calculate the differential conductance across the junction using the Blonder-Tinkham-Klapwijk formula [58]

$$G(E) = G_0 \int_{-K(E)}^{K(E)} \frac{\mathrm{d}k_y}{2K(E)} [1 + |a_L(k_y, E)|^2 - |b_L(k_y, E)|^2], \qquad (4)$$

where a_L and b_L denote the amplitudes of Andreev [60] and normal reflections, respectively. The factor $K(E) = \sqrt{2m_\mathrm{N}(E + \mu)}$ is the maximal value of k_y for a given incident energy E, and $G_0 = 2e^2 KW/(\pi h)$ is the conductance of the metallic lead with width W in the y direction. The microscopic analysis of the scattering amplitudes appears below; cf. Eq. (5). Using formula (4), we calculate the conductance for s- and p-wave superconductors for vanishing barrier ($Z = 0$) and strong barrier ($Z = 4$); see Figs. 1(b) and 1(c), respectively. The case of a vanishing or weak barrier shows the same conductance behavior for both the s- and p-wave case, namely strong oscillations with an energy-dependent period $\delta(E)$. The oscillations come from constructive interference of multiple scattering paths inside the superconducting cavity, where electronic modes in the outer branch of the band structure scatter to hole modes in the inner part of the band structure. Therefore, it is possible to analytically obtain the position of each peak in the conductance, as well as their period, by solving the following interference condition $k_x^{e/h}(E) - k_x^{h/e}(E) = 2\pi n/L$, where n is an integer. This limit of vanishing barriers is studied in detail in Refs. [46,61]. On the other hand, in the opposite limit of strong barriers [cf. the $Z = 4$ case in Fig. 1(c)], the conductance oscillations drastically differ between the s- and p-wave cases. Specifically, they are

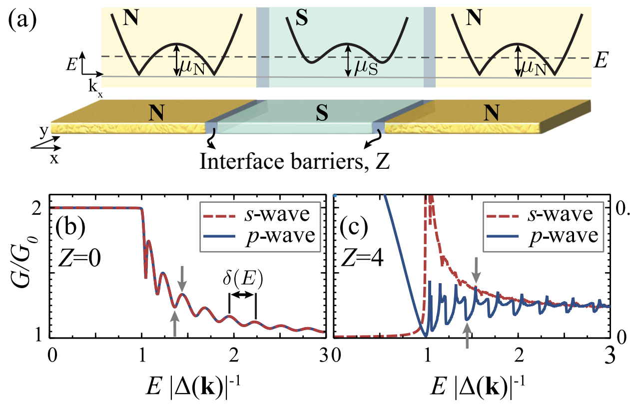

FIG. 1. (a) Sketch of the NSN junction consisting of a superconductor (S) coupled to two normal metal leads (N) with the interface barrier Z. Top panels: quasiparticle dispersion for $k_y = 0$ in all three regions. We consider an incident particle from the left lead with energy E (dashed line). (b) Differential conductance as a function of energy for both the s- and p-wave superconductors in the absence of barriers ($Z = 0$) and with the magnitude of the pair potential set to be equal, i.e., $|\Delta(\mathbf{k})| = \Delta_s = \Delta_p k_F$. The period of the conductance oscillations, $\delta(E)$, increases with energy. (c) Same as (b) in the presence of finite barriers with equal strengths $Z = 4$. Small gray arrows denote the minimum and the maximum of a single oscillation that we use in Fig. 3 when calculating the averaged visibility. For (b) and (c), we used the following parameters: $L = 10\xi_0$, $k_F = 2000\xi_0^{-1}$, $\mu_S = \mu_N = 1000|\Delta(\mathbf{k})|$, where $|\Delta(\mathbf{k})|$ is the magnitude of the pair potential and ξ_0 is the superconducting coherence length.

suppressed in the former and significantly enhanced in the latter. This signature in bulk transport above the gap is the main result of our work and it can be used to distinguish between different types of superconductors.

Momentum-resolved transmission.—To understand the microscopic origin of the results shown in Figs. 1(b) and 1(c), we turn to the analysis of the momentum-resolved transmission probability $T(k_y, E) = 1 + |a_L(k_y, E)|^2 - |b_L(k_y, E)|^2$, i.e., the integrand of Eq. (4), which describes the transmission of charge in the left lead. We start by formulating the junction's scattering equations by considering an electron incident from the left lead with energy E and transverse momentum k_y. We describe the states in the left and right metallic leads (L, R) and the superconducting region (S)

$$\Psi_L = \left[\vec{\Phi}_N^e e^{iq_x^e x} + a_L \vec{\Phi}_N^h e^{iq_x^h x} + b_L \vec{\Phi}_N^e e^{-iq_x^e x}\right] e^{ik_y y},$$
$$\Psi_R = \left[a_R \vec{\Phi}_N^h e^{-iq_x^h x} + b_R \vec{\Phi}_N^e e^{iq_x^e x}\right] e^{ik_y y},$$
$$\Psi_S = \sum_{\eta=\pm} \left[s_\eta^e \vec{\Phi}_S^e e^{i\eta k_x^e x} + s_\eta^h \vec{\Phi}_S^h e^{-i\eta k_x^h x}\right] e^{ik_y y}, \quad (5)$$

where $q_x^{e/h}$ and $k_x^{e/h}$ are the x components of the quasiparticle's momentum in the metallic leads and the superconductor, respectively. In the metallic leads, the spinors $\vec{\Phi}_N^e = (1, 0)^T$, $\vec{\Phi}_N^h = (0, 1)^T$ describe an electron in the outer dispersion branch and a hole in the inner dispersion branch, respectively. $\vec{\Phi}_S^e = [u(k_x^e, k_y), v(k_x^e, k_y)]^T$ and $\vec{\Phi}_S^h = [u(k_x^h, k_y), v(k_x^h, k_y)]^T$ are spinors of electron- and holelike quasiparticles in the superconductor and u, v are electron and hole wave components. The coefficients a_L, a_R, b_L, b_R denote the amplitudes of Andreev reflection [60], cross Andreev reflection, normal reflection, and elastic cotunneling, respectively. The coefficients $s_\pm^{e,h}$ are scattering amplitudes inside the superconductor.

To find the scattering amplitudes above, we impose the following boundary conditions on the two N-S interfaces: $\Psi_{L/R} = \Psi_S$ and $\partial_x \Psi_S - \partial_x \Psi_{L/R} = \pm 2Zk_F \Psi_S$ for the s-wave superconductor, and $\Psi_{L/R} = \Psi_S$ and $\partial_x \Psi_S - \partial_x \Psi_{L/R} = \pm 2Zk_F \Psi_S + (m\Delta/\hbar)\sigma_x \Psi_S$ for the p-wave superconductor, where "±" corresponds to the left and right interfaces at $x = 0, L$, respectively. Note that due to the perfectly flat barriers in y direction, the momentum k_y is preserved for all scattering processes.

We solve the scattering equations (5), with the aforementioned boundary conditions, for a_L and b_L, and show the result for $T(k_y, E)$ in Fig. 2 for both the s- and p-wave superconductors and in the limits of weak [Figs. 2(a) and 2(b)] and strong [Figs. 2(c)–2(f)] barriers. In the former, $T(k_y, E)$ is identical for s- and p-wave superconductors and we identify two main features (marked ① and ② in the figure). In region ①, the energy resides in the superconducting gap, i.e., the *main gap* [see Figs. 1(a) and 1(b)], and the transmission through the NSN junction is constant and equal to 2 without the effect of the interface barriers [58,60]. In region ②, both electron- and holelike modes coexist; due to the predominant electron-to-hole scattering, the transmission maxima exhibit a relatively weak dependence on k_y. Consequently, strong oscillations manifest in the conductance; see Fig. 1(b). Note that $T(k_y, E) = T(-k_y, E)$, and therefore in Fig. 2, we show only positive k_y plane.

In the opposite limit of strong barriers—or equivalently, weak coupling to the leads—the transmission throughout region ① is now strongly suppressed for the s-wave superconductor, with a power-law scaling with Z [58]. At the same time, for the p-wave superconductor on top of the suppressed transmission, a clear sign of a topological edge mode, marked with ③, can be seen [11]. On the other hand, the maxima of $T(k_y, E)$ in region ② become sharper for both s-wave and p-wave superconductors and they also acquire an additional structure that was smeared out by the strong coupling with the leads; see Figs. 2(c)–2(f). Moreover, gaps between maxima—dubbed "secondary gaps"—close in the case of the s-wave superconductor, while in the p-wave case they remain open even for very large barrier strengths Z, as marked by ④ in Figs. 2(e) and 2(f).

Opening of secondary gaps.—To better understand the mechanisms responsible for the different behavior of the

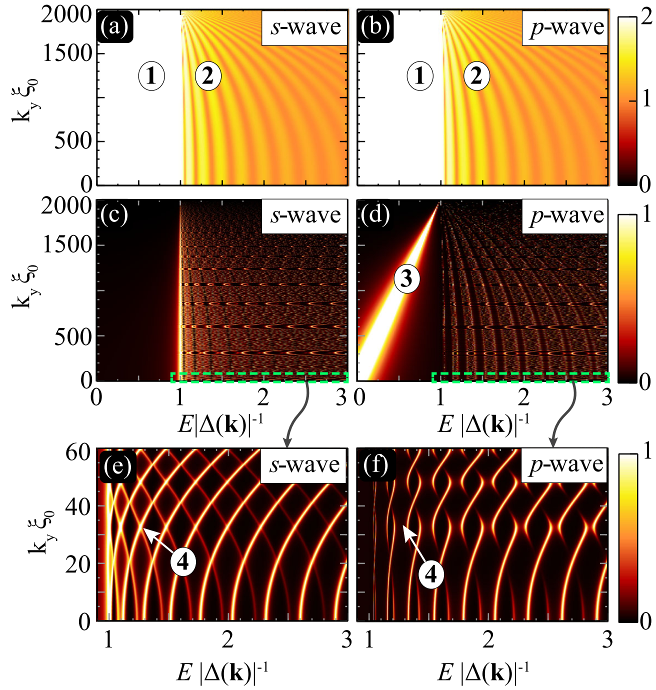

FIG. 2. (a),(b) Transmission probability with $Z = 0$ for s- and p-wave superconductors, respectively. Two main features are visible: ① inside the gap, perfect transmission occurs with $T = 2$, and ② both electron- and holelike quasiparticles are present, hybridize with one another, and produce oscillations that only weakly depend on k_y. (c),(d) Transmission probability with $Z = 2$ for s- and p-wave superconductors, respectively. In (d) the topological in-gap mode, marked with ③, is visible, while in (c) there are no in-gap modes present. (e),(f) The enlarged regions of (c) and (d). A new differentiating feature, marked with ④, appears in a case of strong barriers: in (e), the transmission maxima of different electron- and holelike modes cross, while in (f) avoided crossings appear, leading to secondary gaps and flat transmission bands appear. For all plots, we used the same parameters as in Fig. 1.

secondary gaps in transmission—and with that the difference in conductance oscillations—between the s- and p-wave superconductors, we employ a perturbative approach. We first concentrate on the limit of strong barriers. In this limit, the gap structure in the transmission plots [cf. Figs. 2(c)–2(f)] is determined by the eigenmodes of the superconducting cavity, which are only perturbatively affected by the coupling to the leads. Therefore, it is sufficient to analyze the isolated superconductor, which is finite in the x direction with length L and infinite in the y direction. Doing so, we discover that the momentum dependence of the pairing potential in Eq. (3) is responsible for the selective hybridization of particle- and holelike modes of the cavity; see Supplemental Material [62] for more details. Crucially, in the p-wave superconductor, secondary gaps are opened even without the presence of the leads due to the k_x dependence of the pairing term in H_S. The Hamiltonian of the s-wave superconductor, on the other hand, has constant off-diagonal elements and the particle- and holelike modes do not hybridize. As a result, the secondary gaps in $T(k_y, E)$ are closed in that case.

In the limit of weak barriers, i.e., the strong hybridization with the leads, secondary gaps are opened for both s-wave and p-wave superconductors; see Figs. 2(a) and 2(b). To understand this, we include the leads in our analytical analysis via the weak tunnel coupling to the superconductor. Such treatment, which relies on a calculation of the self-energy, gives rise to the finite coupling between the electron- and holelike modes of the superconductor, which is second-order in the tunneling. As a result, secondary gaps are opened between all degenerate modes of the closed cavity; see Supplemental Material [62] for details. This conclusion is also valid when the tunnel coupling is strong, i.e., when there are no barriers at all; cf. Figs. 2(a) and 2(b).

To quantify the impact of the barrier in both s- and p-wave cases, we study the visibility of conductance oscillations defined as

$$\nu = \frac{1}{N}\sum_{i=1}^{N}\frac{G_i^{\max} - G_i^{\min}}{G_i^{\max} + G_i^{\min}}, \qquad (6)$$

where $G_i^{\max}$ and $G_i^{\min}$ are the neighboring local maximum and minimum values of the conductance; see gray arrows in Figs. 1(b) and 1(c). We numerically calculate the visibility of the first five periods of oscillation ($N = 5$) as a function of the barrier strength Z; see Fig. 3. While in the absence of the barriers, $Z = 0$, both types of superconductors have the same values of visibility: at large Z the visibility increases with Z for the p-wave superconductor and saturates to a small constant for the s-wave superconductor. Such behavior reflects the analytical discussion above on secondary gaps. Note that when $Z > 2$ in the s-wave case [dashed lines in Fig. 3(a)], the height of the conductance oscillations is so small that it becomes comparable to fluctuations

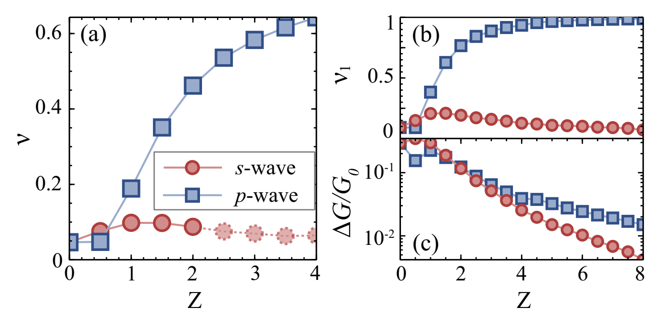

FIG. 3. (a) Visibility of the conductance oscillations defined in Eq. (6) as a function of the barrier strength for the s-wave (red dots) and the p-wave (blue squares) cases. (b) Visibility of the first oscillation, i.e., the one closest to the gap for both s- and p-wave cases. (c) The height of the first oscillation, $\Delta G \equiv G_1^{\max} - G_1^{\min}$, for both cases. We used the same parameters as in Fig. 1.

caused by the finite-element numerical integration over Eq. (4). On the other hand, the height of the first oscillation is distinguishable for much larger Z in both the s- and p-wave cases. We plot the visibility of that first oscillation peak in Fig. 3(b), from which the same trend can be extracted as in Fig. 3(a). Lastly, in Fig. 3(c), we plot the height of the aforementioned first oscillation—defined as $\Delta G \equiv G_1^{\max} - G_1^{\min}$—for both cases. The height decays for large Z, but with a slower rate in the p-wave case.

In conclusion, we have demonstrated that Tomasch oscillations of Bogoliubov quasiparticles provide a promising method to distinguish between topological p-wave superconductivity and conventional s-wave superconductivity. Specifically, the resulting conductance oscillations display contrasting behavior for the two types of superconductors as the interface barriers increase, which is a direct manifestation of the pairing symmetries. Our study introduces bulk probes for identifying topological superconductivity, which is usually overlooked. Our proposed above-gap transport signature can serve as an essential supplement to in-gap measurements [62]. Interestingly, Tomasch oscillations were first reported approximately 60 years ago in both Pb and In films with thicknesses ranging from 3 to 30 μm [49,50], making their observation in junctions with topological superconductors highly promising using state-of-the-art techniques. Furthermore, some recent experiments on junctions made of a normal metal, an insulator, and a superconductor [70] reported high tunability of the barrier strength Z. By changing the thickness of the barrier, Z is easily tuned to $Z \gg 10$, which lies deeply in the regime that we discuss in our work. Last, our mechanism is established for continuum single-band models without the presence of spin-orbit coupling, where the band inversion and pairing mechanism dictate the appearance of topology; it would be interesting to extend the discussion to more complicated multiband systems as well as lattice models with anisotropy. There, anisotropy can cause a significant morphing of the sombrero-shaped band structure, which can even lead to topological phase transitions by gap closing at momenta away from the Γ point [71]. Whether our method can be applied to distinguish between different phases in that case will be the focus of future work.

All data that support the plots within this Letter are available from the corresponding author upon request.

We are grateful to W. Belzig for insightful discussions. W. C. acknowledges financial support from the National Natural Science Foundation of China under Grants No. 12074172 and No. 12222406, and the National Key Projects for Research and Development of China under Grant No. 2022YFA120470. X. R. C. acknowledges financial support from the National Natural Science Foundation of China under Grant No. 12304064. D. Y. X. acknowledges financial support from the State Key Program for Basic Research of China under Grant No. 2021YFA1400403. A. Š. acknowledges financial support from the Swiss National Science Foundation (Grant No. 199969). O. Z. acknowledges financial support from the Deutsche Forschungsgemeinschaft (DFG)—Project No. 449653034.

*These authors contributed equally to this work.
†Corresponding author: pchenweis@gmail.com
‡Present address: Department of Physics, Faculty of Science, University of Zagreb, Zagreb, Croatia.

[1] J. Bardeen, L. N. Cooper, and J. R. Schrieffer, Theory of superconductivity, Phys. Rev. **108**, 1175 (1957).
[2] M. Sigrist and K. Ueda, Phenomenological theory of unconventional superconductivity, Rev. Mod. Phys. **63**, 239 (1991).
[3] A. P. Mackenzie and Y. Maeno, The superconductivity of Sr_2RuO_4 and the physics of spin-triplet pairing, Rev. Mod. Phys. **75**, 657 (2003).
[4] M. Z. Hasan and C. L. Kane, Colloquium: Topological insulators, Rev. Mod. Phys. **82**, 3045 (2010).
[5] X.-L. Qi and S.-C. Zhang, Topological insulators and superconductors, Rev. Mod. Phys. **83**, 1057 (2011).
[6] Y. Tanaka, M. Sato, and N. Nagaosa, Symmetry and topology in superconductors–odd-frequency pairing and edge states–, J. Phys. Soc. Jpn. **81**, 011013 (2012).
[7] M. Sato and Y. Ando, Topological superconductors: A review, Rep. Prog. Phys. **80**, 076501 (2017).
[8] J. G. Bednorz and K. A. Müller, Possible high T_c superconductivity in the Ba-La-Cu-O system, Z. Phys. B Condens. Matter **64**, 189 (1986).
[9] L. Fu and C. L. Kane, Superconducting proximity effect and Majorana fermions at the surface of a topological insulator, Phys. Rev. Lett. **100**, 096407 (2008).
[10] M. Leijnse and K. Flensberg, Introduction to topological superconductivity and Majorana fermions, Semicond. Sci. Technol. **27**, 124003 (2012).
[11] B. A. Bernevig and T. L. Hughes, *Topological Insulators and Topological Superconductors* (Princeton University Press, Princeton, NJ, 2013).
[12] A. Y. Kitaev, Unpaired Majorana fermions in quantum wires, Phys. Usp. **44**, 131 (2001).
[13] A. M. Lobos and S. D. Sarma, Tunneling transport in NSN Majorana junctions across the topological quantum phase transition, New J. Phys. **17**, 065010 (2015).
[14] G. E. Volovik, Fermion zero modes on vortices in chiral superconductors, JETP Lett. **70**, 609 (1999).
[15] N. Read and D. Green, Paired states of fermions in two dimensions with breaking of parity and time-reversal symmetries and the fractional quantum Hall effect, Phys. Rev. B **61**, 10267 (2000).
[16] D. A. Ivanov, Non-Abelian statistics of half-quantum vortices in P-wave superconductors, Phys. Rev. Lett. **86**, 268 (2001).
[17] R. R. Biswas, Majorana fermions in vortex lattices, Phys. Rev. Lett. **111**, 136401 (2013).
[18] H.-H. Sun, K.-W. Zhang, L.-H. Hu, C. Li, G.-Y. Wang, H.-Y. Ma, Z.-A. Xu, C.-L. Gao, D.-D. Guan, Y.-Y. Li, C.

Liu, D. Qian, Y. Zhou, L. Fu, S.-C. Li, F.-C. Zhang, and J.-F. Jia, Majorana zero mode detected with spin selective Andreev reflection in the vortex of a topological superconductor, Phys. Rev. Lett. **116**, 257003 (2016).

[19] J. Li, T. Neupert, Z. Wang, A. H. MacDonald, A. Yazdani, and B. A. Bernevig, Two-dimensional chiral topological superconductivity in Shiba lattices, Nat. Commun. **7**, 12297 (2016).

[20] C. Brun, T. Cren, and D. Roditchev, Review of 2d superconductivity: The ultimate case of epitaxial monolayers, Semicond. Sci. Technol. **30**, 013003 (2016).

[21] A. Kitaev, Fault-tolerant quantum computation by anyons, Ann. Phys. (Amsterdam) **303**, 2 (2003).

[22] C. Nayak, S. H. Simon, A. Stern, M. Freedman, and S. Das Sarma, Non-Abelian anyons and topological quantum computation, Rev. Mod. Phys. **80**, 1083 (2008).

[23] J. Alicea, Y. Oreg, G. Refael, F. von Oppen, and M. P. A. Fisher, Non-Abelian statistics and topological quantum information processing in 1d wire networks, Nat. Phys. **7**, 412 (2011).

[24] T. M. Rice and M. Sigrist, Sr_2RuO_4: An electronic analogue of 3He?, J. Phys. Condens. Matter **7**, L643 (1995).

[25] G. Baskaran, Why is Sr_2 Ru O_4 not a high T_c superconductor? Electron correlation, Hund's coupling and p-wave instability, Physica (Amsterdam) **223-224B**, 490 (1996).

[26] M. Sigrist, Review on the chiral p-wave phase of Sr_2RuO_4, Prog. Theor. Phys. Suppl. **160**, 1 (2005).

[27] L. Jiao, S. Howard, S. Ran, Z. Wang, J. O. Rodriguez, M. Sigrist, Z. Wang, N. P. Butch, and V. Madhavan, Chiral superconductivity in heavy-fermion metal UTe_2, Nature (London) **579**, 523 (2020).

[28] W. Qin, J. Gao, P. Cui, and Z. Zhang, Two-dimensional superconductors with intrinsic p-wave pairing or nontrivial band topology, Sci. China Phys. Mech. Astron. **66**, 267005 (2023).

[29] G. C. Ménard, S. Guissart, C. Brun, R. T. Leriche, M. Trif, F. Debontridder, D. Demaille, D. Roditchev, P. Simon, and T. Cren, Two-dimensional topological superconductivity in Pb/Co/Si(111), Nat. Commun. **8**, 2040 (2017).

[30] R. M. Lutchyn, J. D. Sau, and S. Das Sarma, Majorana fermions and a topological phase transition in semiconductor-superconductor heterostructures, Phys. Rev. Lett. **105**, 077001 (2010).

[31] Y. Oreg, G. Refael, and F. von Oppen, Helical liquids and Majorana bound states in quantum wires, Phys. Rev. Lett. **105**, 177002 (2010).

[32] J. Klinovaja, P. Stano, A. Yazdani, and D. Loss, Topological superconductivity and Majorana fermions in RKKY systems, Phys. Rev. Lett. **111**, 186805 (2013).

[33] C. Beenakker and L. Kouwenhoven, A road to reality with topological superconductors, Nat. Phys. **12**, 618 (2016).

[34] J. L. Lado and M. Sigrist, Two-dimensional topological superconductivity with antiferromagnetic insulators, Phys. Rev. Lett. **121**, 037002 (2018).

[35] Y. Volpez, D. Loss, and J. Klinovaja, Second-order topological superconductivity in π-junction Rashba layers, Phys. Rev. Lett. **122**, 126402 (2019).

[36] M. Sato, Y. Takahashi, and S. Fujimoto, Non-Abelian topological order in *s*-wave superfluids of ultracold fermionic atoms, Phys. Rev. Lett. **103**, 020401 (2009).

[37] J. D. Sau, R. M. Lutchyn, S. Tewari, and S. Das Sarma, Generic new platform for topological quantum computation using semiconductor heterostructures, Phys. Rev. Lett. **104**, 040502 (2010).

[38] J. Alicea, Majorana fermions in a tunable semiconductor device, Phys. Rev. B **81**, 125318 (2010).

[39] V. Mourik, K. Zuo, S. M. Frolov, S. R. Plissard, E. P. A. M. Bakkers, and L. P. Kouwenhoven, Signatures of Majorana fermions in hybrid superconductor-semiconductor nanowire devices, Science **336**, 1003 (2012).

[40] A. Das, Y. Ronen, Y. Most, Y. Oreg, M. Heiblum, and H. Shtrikman, Zero-bias peaks and splitting in an Al–InAs nanowire topological superconductor as a signature of Majorana fermions, Nat. Phys. **8**, 887 (2012).

[41] S. M. Albrecht, A. P. Higginbotham, M. Madsen, F. Kuemmeth, T. S. Jespersen, J. Nygård, P. Krogstrup, and C. M. Marcus, Exponential protection of zero modes in Majorana islands, Nature (London) **531**, 206 (2016).

[42] P. de Gennes, *Superconductivity of Metals and Alloys*, Advanced book classics (W.A. Benjamin, New York, 1966).

[43] M. Altarelli, Electronic structure and semiconductor-semimetal transition in InAs-GaSb superlattices, Phys. Rev. B **28**, 842 (1983).

[44] M. J. Yang, C. H. Yang, B. R. Bennett, and B. V. Shanabrook, Evidence of a hybridization gap in "semimetallic" InAs/GaSb systems, Phys. Rev. Lett. **78**, 4613 (1997).

[45] M. Lakrimi, S. Khym, R. J. Nicholas, D. M. Symons, F. M. Peeters, N. J. Mason, and P. J. Walker, Minigaps and novel giant negative magnetoresistance in InAs/GaSb semimetallic superlattices, Phys. Rev. Lett. **79**, 3034 (1997).

[46] M. Karalic, A. Štrkalj, M. Masseroni, W. Chen, C. Mittag, T. Tschirky, W. Wegscheider, T. Ihn, K. Ensslin, and O. Zilberberg, Electron-hole interference in an inverted-band semiconductor bilayer, Phys. Rev. X **10**, 031007 (2020).

[47] Y. Zhao, A. Leuch, O. Zilberberg, and A. Štrkalj, Electron optics using negative refraction in two-dimensional inverted-band *pn* junctions, Phys. Rev. B **108**, 195301 (2023).

[48] Y.-Q. Li, X.-R. Chen, W. Luo, T. Zhou, and W. Chen, Fabry-Pérot interference in 2D low-density Rashba gas, Europhys. Lett. **137**, 36003 (2022).

[49] W. J. Tomasch, Geometrical resonance in the tunneling characteristics of superconducting Pb, Phys. Rev. Lett. **15**, 672 (1965).

[50] W. J. Tomasch, Geometrical resonance and boundary effects in tunneling from superconducting In, Phys. Rev. Lett. **16**, 16 (1966).

[51] W. L. McMillan and P. W. Anderson, Theory of geometrical resonances in the tunneling characteristics of thick films of superconductors, Phys. Rev. Lett. **16**, 85 (1966).

[52] W. L. McMillan, Theory of superconductor—normal-metal interfaces, Phys. Rev. **175**, 559 (1968).

[53] C. G. Granqvist and T. Claeson, Superconductivity in ultrathin films II. Structure in tunneling curves, Phys. Condens. Matter **18**, 99 (1974).

[54] P. Nédellec, L. Dumoulin, and E. Guyon, Tomasch effect and superconducting proximity, J. Low Temp. Phys. **24**, 663 (1976).

[55] A. Kononov, O. O. Shvetsov, S. V. Egorov, A. V. Timonina, N. N. Kolesnikov, and E. V. Deviatov, Signature of Fermi arc surface states in Andreev reflection at the WTe_2 Weyl semimetal surface, Europhys. Lett. **122**, 27004 (2018).

[56] T. H. Kokkeler, A. A. Golubov, and B. J. Geurts, Testing superconducting pairing symmetry in multiterminal junctions, Semicond. Sci. Technol. **35**, 084005 (2022).

[57] Note that the Hamiltonian in the s-wave case is written in the basis $(d_{k,\sigma}, d^{\dagger}_{-k,-\sigma})^T$ with $\sigma = (\uparrow, \downarrow)$, and the one for the p-wave case has a spinless basis $(d_k, d^{\dagger}_{-k})^T$, where d and $d^{\dagger}$ are the electron annihilation and creation operator, respectively.

[58] G. E. Blonder, M. Tinkham, and T. M. Klapwijk, Transition from metallic to tunneling regimes in superconducting microconstrictions: Excess current, charge imbalance, and supercurrent conversion, Phys. Rev. B **25**, 4515 (1982).

[59] E. Scheer, W. Belzig, Y. Naveh, M. H. Devoret, D. Esteve, and C. Urbina, Proximity effect and multiple Andreev reflections in gold atomic contacts, Phys. Rev. Lett. **86**, 284 (2001).

[60] A. F. Andreev, The thermal conductivity of the intermediate state in superconductors, Sov. Phys. JETP **19**, 1228 (1964).

[61] A. Štrkalj, Coherent effects in transport through open many-body one-dimensional systems, Ph.D. thesis, Eidgenössische Technische Hochschule Zürich, Switzerland, 2021.

[62] See Supplemental Material at http://link.aps.org/supplemental/10.1103/PhysRevLett.132.066301, which includes Refs. [3,46,61,63–69], for the discussions on the opening of secondary gaps in an isolated superconducting cavity for the p-wave pairing and similar gap opening due to the coupling to the leads for the s-wave pairing, discussion of the length dependence of the periodicity of oscillations, and a short remark on clear advantages and drawbacks of using Tomasch oscillations to probe topological superconductivity.

[63] C. Caroli, P. De Gennes, and J. Matricon, Bound fermion states on a vortex line in a Type II superconductor, Phys. Lett. **9**, 307 (1964).

[64] E. Prada, P. San-Jose, M. W. A. de Moor, A. Geresdi, E. J. H. Lee, J. Klinovaja, D. Loss, J. Nygård, R. Aguado, and L. P. Kouwenhoven, From Andreev to Majorana bound states in hybrid superconductor–semiconductor nanowires, Nat. Rev. Phys. **2**, 575 (2020).

[65] Y. Luh, Bound state in superconductors with paramagnetic impurities, Acta Phys. Sin. **21**, 75 (1965).

[66] H. Shiba, Classical spins in superconductors, Prog. Theor. Phys. **40**, 435 (1968).

[67] A. Rusinov, Superconductivity near a paramagneticimpurity, Sov. Phys. JETP **9**, 85 (1969).

[68] D. J. Van Harlingen, Phase-sensitive tests of the symmetry of the pairing state in the high-temperature superconductors—evidence for $d_{x^2-y^2}$ symmetry, Rev. Mod. Phys. **67**, 515 (1995).

[69] K. D. Nelson, Z. Q. Mao, Y. Maeno, and Y. Liu, Odd-parity superconductivity in Sr_2RuO_4, Science **306**, 1151 (2004).

[70] Q. Cao, E. J. Telford, A. Benyamini, I. Kennedy, A. Zangiabadi, K. Watanabe, T. Taniguchi, C. R. Dean, and B. M. Hunt, Tunneling spectroscopy of two-dimensional materials based on via contacts, Nano Lett. **22**, 8941 (2022).

[71] M. Sato, Topological odd-parity superconductors, Phys. Rev. B **81**, 220504(R) (2010).